



## Development of Potent Inhibitors of the Mycobacterium tuberculosis Virulence Factor Zmp1 and Evaluation of Their Effect on Mycobacterial Survival inside Macrophages

This is the peer reviewed version of the following article:

*Original:*

Paolino, M., Brindisi, M., Vallone, A., Butini, S., Campiani, G., Nannicini, C., et al. (2018). Development of Potent Inhibitors of the Mycobacterium tuberculosis Virulence Factor Zmp1 and Evaluation of Their Effect on Mycobacterial Survival inside Macrophages. CHEMMEDCHEM, 13(5), 422-430 [10.1002/cmdc.201700759].

*Availability:*

This version is available <http://hdl.handle.net/11365/1035556> since 2018-03-22T12:28:48Z

*Published:*

DOI:10.1002/cmdc.201700759

*Terms of use:*

Open Access

The terms and conditions for the reuse of this version of the manuscript are specified in the publishing policy. Works made available under a Creative Commons license can be used according to the terms and conditions of said license.

For all terms of use and more information see the publisher's website.

(Article begins on next page)

# Development of potent inhibitors of the *Mycobacterium tuberculosis* virulence factor Zmp1 and evaluation of their effect on mycobacterial survival inside macrophages

Marco Paolino,<sup>[†,a]</sup> Margherita Brindisi,<sup>[†,a]</sup> Alessandra Vallone,<sup>[a]</sup> Stefania Butini,<sup>[a]</sup> Giuseppe Campiani,<sup>[a]</sup> Chiara Nannicini,<sup>[a]</sup> Germano Giuliani,<sup>[a]</sup> Maurizio Anzini,<sup>[a]</sup> Stefania Lamponi,<sup>[a]</sup> Gianluca Giorgi,<sup>[a]</sup> Diego Sbardella,<sup>[b]</sup> Davide M. Ferraris,<sup>[c]</sup> Stefano Marini,<sup>[b]</sup> Massimo Coletta,<sup>[b]</sup> Ivana Palucci,<sup>[d]</sup> Mariachiara Minerva,<sup>[d]</sup> Giovanni Delogu,<sup>[d]</sup> Ilaria Pepponi,<sup>[e]</sup> Delia Goletti,<sup>[e]</sup> Andrea Cappelli,<sup>[a]\*</sup> Sandra Gemma,<sup>[a]\*</sup> Simone Brogi<sup>[a]</sup>

- [a] Dr M. Paolino, Dr. M. Brindisi, Dr. A. Vallone, Prof. S. Butini, Prof. G. Campiani, Dr. C. Nannicini, Dr. G. Giuliani, Prof. M. Anzini, Dr. S. Lamponi, Prof. G. Giorgi, Prof. A. Cappelli, Prof. S. Gemma, Dr. S. Brogi  
European Research Centre for Drug Discovery and Development –NatSynDrugs- and Department of Biotechnology, Chemistry, and Pharmacy  
University of Siena  
via Aldo Moro 1, 53100 Siena, Italy  
E-mail: [gemma@unisi.it](mailto:gemma@unisi.it); [andrea.cappelli@unisi.it](mailto:andrea.cappelli@unisi.it)  
†These authors contributed equally
- [b] Prof. D. Sbardella, Prof. S. Marini, Prof. M. Coletta  
Department of Clinical Sciences and Translational Medicine  
University of Roma Tor Vergata, Via Montpellier 1, I-00133 Roma, Italy
- [c] Dr. D. M. Ferraris  
Department of Chemical, Food, Pharmaceutical and Pharmacological Sciences  
University of Piemonte Orientale “Amedeo Avogadro”, Largo Donegani 2, I-28100 Novara, Italy
- [d] Dr. I. Palucci, Dr M. Minerva, Prof. G. Delogu  
Institute of Microbiology  
Università Cattolica del Sacro Cuore – Fondazione Policlinico Universitario Gemelli, Rome, Italy, Largo A. Gemelli, 8 – 00168 Rome, Italy
- [e] Dr I. Pepponi, Dr. D. Goletti  
Translational Research Unit  
National Institute for Infectious Diseases (INMI) “L. Spallanzani”, Via Portuense, 292, 00149 Roma, Italy

Supporting information for this article is given via a link at the end of the document

**Abstract:** The enzyme Zmp1 is a zinc-peptidase having a critical role in *M. tuberculosis* pathogenicity. Here we describe the identification of a small set of Zmp1 inhibitors based on a novel 8-hydroxyquinoline-2-hydroxamate scaffold. Among the synthesized compounds, **1c** was the most potent Zmp1 inhibitor known to date, and its binding mode was analysed both through kinetic studies and molecular modelling, identifying critical interactions of **1c** with the zinc-ion and residues in the active site. Effect of **1c** on intracellular *Mycobacterium* survival was assayed in J774 murine macrophages infected with *M. tuberculosis* H37Rv or *M. bovis* BCG and human monocyte-derived macrophages infected with *M. tuberculosis* H37Rv. Cytotoxicity and genotoxicity were also assessed. Overall, inhibitor **1c** displayed interesting in vitro antitubercular properties worth of further investigation.

## Introduction

Tuberculosis (TB) is a disease caused by the facultative intracellular bacterium *Mycobacterium tuberculosis* (*M. tuberculosis*). According to the World Health Organization (WHO) data, TB affected 10.4 million people in 2015, and 1.2 million people were co-infected with the human immunodeficiency virus (HIV).<sup>[1]</sup> One of the main public health challenges regarding TB is the diffusion of multi-drug resistant (MDR)- and extensively drug resistant (XDR)-TB infections.<sup>[2]</sup> Despite the recent new tools in TB therapy, i.e. delamanid and bedaquiline,<sup>[3, 4]</sup> safer and more

effective drugs with innovative mechanisms of action are urgently required to increase our armamentarium against MDR-TB. *M. tuberculosis* evolved several virulence factors that can interfere with the host immune response to infection.<sup>[5]</sup> Among them, it has been demonstrated that the virulence factor Zmp1, a Zn<sup>2+</sup>-metalloprotease essential for mycobacterial survival in macrophages *in vitro*, interferes with the phagosome maturation by inhibiting the inflammasome.<sup>[6, 7]</sup> This allows the bacterium to survive in the phagosome and prevents fusion of the phagosome with the lysosome. Although some findings were later debated,<sup>[8]</sup> Zmp1 plays a key role in *M. tuberculosis* pathogenicity and therefore is worth of further investigation as a putative drug target.<sup>[9-11]</sup>

Zinc-peptidases are classically inhibited by molecules incorporating a zinc binding group (ZBG) able to coordinate the active site metal ion, and responsible for high-affinity and inhibitory potency. The vast majority of zinc-peptidase inhibitors reported to date contains a hydroxamic acid as the ZBG, although a number of heterocyclic-based ZBGs have also been identified.<sup>[12]</sup> Among them, the 8-hydroxyquinoline system attracted our attention since it is a privileged structure and has been used as metal-interacting group for a range of pharmacological applications.<sup>[13]</sup> In order to identify potent and drug-like Zmp1 inhibitors, we designed a novel ZBG by hybridizing the 8-hydroxyquinoline ring with a hydroxamate moiety (Figure 1, compounds **1a-e**). For evaluating structure-activity relationships, we also prepared the isosteric analogues **2a,b**, lacking the hydroxamate oxygen, and compounds **5a,b**

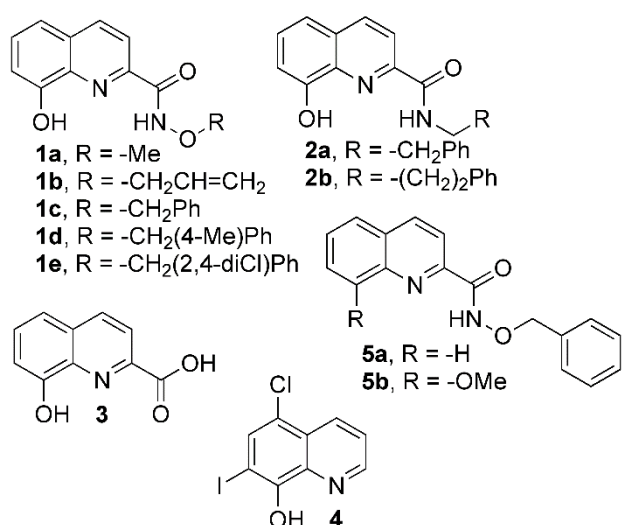


**Figure 1.** Structures of 8-hydroxyquinoline-derivatives **1a-e**, **2a,b**, **3**, **4** and **5a,b** investigated as Zmp1 inhibitors.

lacking the free 8-hydroxy group. The activity of the novel chemical entities was also compared to clioquinol (5-chloro-7-iodo-quinolin-8-ol, **4**), a compound that is able to interact with Zn ion but lacking the hydrophobic pendant side chain. Derivatives **5a,b** were designed to investigate the role of the hydroxyl group at C8. We identified the potent Zmp1 inhibitor **1c** (Figure 1), we characterized its kinetics of inhibition and mode of binding (through extensive computational studies) and evaluated the growth of *M. tuberculosis* H37Rv inside both human and murine macrophages *in vitro*.

## Results and discussion

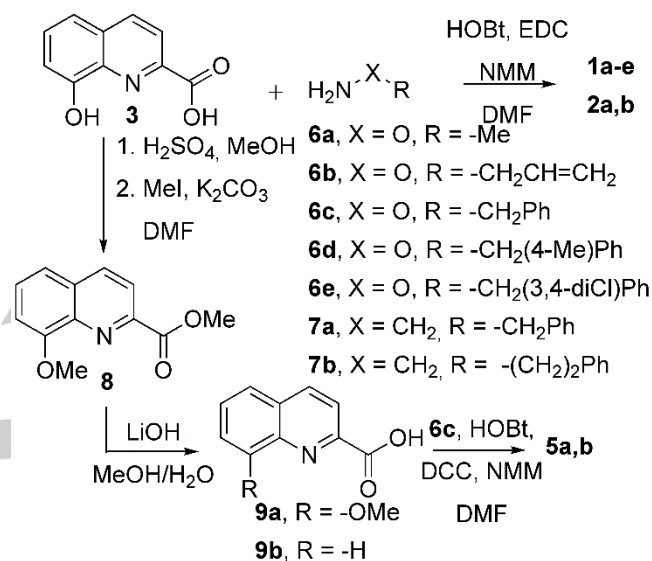
### Chemistry

Compounds **1a-e**, **2a,b** and **5a,b** were synthesized as described in Scheme 1 through a straightforward synthetic approach. Coupling of carboxylic acid **3** with commercially available *O*-alkylhydroxylamines **6a-e** or alkylamines **7a,b** under classical coupling conditions afforded target compounds **1a-e** and **2a,b** in good overall yield. The structure of compounds **1b-d** was confirmed by X-ray crystallographic studies (Figures S1-3 of the Supporting Information file). The 8-hydroxyquinoline-2-carboxylic acid **3** was used as the starting material also for the synthesis of compounds **5a**. Accordingly, acid-catalyzed esterification of the carboxylic acid followed by *O*-methylation afforded intermediate **8**. This latter compound was treated with LiOH to release the free carboxylic acid **9a**, which was coupled with **6c** as described above to afford **5a**. Finally, the same coupling procedure was applied to quinoline-2-carboxylic acid **9b** to furnish **5b**.

### Zmp1 inhibitory activity and kinetic analysis

Novel compounds and **4** were tested for their *in vitro* inhibitory activity against Zmp1 by using a fluorimetric assay. The initial

approach was only focused on selecting molecules characterized by the lowest IC<sub>50</sub> (Table 1). Gratifyingly, our design approach led to the discovery of potent, nanomolar inhibitors of Zmp1. To the best of our knowledge, the benzyl-derivative **1c** (IC<sub>50</sub> = 11 nM) is the most potent Zmp1 inhibitor reported to date, compared to a previously reported rhodamine-based inhibitor (K<sub>i</sub> = 94 nM).<sup>[14]</sup> Moreover, we assayed the inhibitory activity of **1c** on other Zn<sup>2+</sup> enzymes, such as the matrix metalloproteinases (MMPs), namely MMP-1 and MMP-2, which belong to the collagenase and gelatinase subgroups, respectively, and are among the most represented Zn<sup>2+</sup> enzymes in human tissues.<sup>[15]</sup> The IC<sub>50</sub> of **1c** on MMP-1 turned out to be >10 μM and that on MMP-2 ≥ 1 μM (data not shown). This result emphasizes the specificity of **1c** in inhibiting Zmp1.



**Scheme 1.** Synthesis of compounds **1a-e**, **2a,b**, and **3a,b**.

**Table 1.** Zmp1 Inhibitory Activity (IC<sub>50</sub>, μM)

Compound	IC <sub>50</sub> (μM)
<b>1a</b>	0.115
<b>1b</b>	0.123
<b>1c</b>	0.011
<b>1d</b>	0.217
<b>1e</b>	0.189
<b>2a</b>	>10
<b>2b</b>	>10
<b>3</b>	>10
<b>5a</b>	>10
<b>5b</b>	>10
Clioquinol ( <b>4</b> )	>50

For the most potent inhibitor **1c**, a detailed kinetic analysis was performed in order to clarify the mechanism of Zmp1

## FULL PAPER

inhibition and calculate the actual  $K_i$ . Enzymatic kinetic data have been obtained, at different concentrations of inhibitor **1c**, as a function of substrate concentration and analyzed according to the following equation:

$$\frac{[E_0]}{v} = \frac{{}^{obs}K_m}{{}^{obs}k_{cat}} \cdot \frac{1}{[S]} + \frac{1}{{}^{obs}k_{cat}} \quad (\text{eq. 1})$$

where  $[E_0]$  is the enzyme concentration,  $v$  is the observed rate (expressed as moles/s),  $[S]$  is the substrate concentration,  ${}^{obs}K_m$  is the observed Michaelis-Menten equilibrium constant (reflecting the enzyme-substrate affinity) and  ${}^{obs}k_{cat}$  is the observed velocity of the rate-limiting step. At each inhibitor **1c** concentration a dependence of Zmp1 enzymatic activity on a fluorogenic substrate S has allowed to obtain a value of  ${}^{obs}K_m$  and  ${}^{obs}k_{cat}$  and Figure 2 shows the dependence of  ${}^{obs}K_m$  (Panel A) and of  ${}^{obs}k_{cat}$  (Panel B) on the inhibitor **1c** concentration. Interestingly, we observed a bimodal behavior, characterized first by a marked increase of  ${}^{obs}K_m$ , as expected for an inhibitory effect, followed by a decrease at higher inhibitor **1c** concentrations (Figure 2A); in the case of  ${}^{obs}k_{cat}$  we only observed a decrease (Figure 2B), which parallels the first  ${}^{obs}K_m$  increase. This behavior underlies the existence of two different binding sites for the molecule; the higher affinity one displays a decrease of substrate affinity (accompanied by a decrease of the rate of substrate cleavage), while the binding of **1c** to the second lower affinity site brings about a (partial) recovery of substrate affinity without affecting the rate of substrate cleavage. The presence in Zmp1 of two binding sites for the

inhibitor **1c** with two differing functional sites is the simplest mechanism to account for the observed behavior in Figures 2A and 2B. Obviously, several other more complex mechanisms might describe this feature, but their use would not be justified by the available structural information; therefore, since the simplest mechanism in Figure 2C seems sufficient to satisfactorily describe the observed data, we have used it throughout our analysis. Therefore, based on Scheme reported in Figure 2C, the dependence of  ${}^{obs}K_m$  on inhibitor **1c** concentration  $[I]$  can be described by Eq. (2a)

$${}^{obs}K_m = {}^0K_m \cdot \frac{K_{I1} \cdot K_{I2} \cdot \alpha \cdot \gamma + K_{I2} \cdot \alpha \cdot \gamma \cdot [I] + \alpha \cdot \gamma \cdot [I]^2}{K_{I1} \cdot K_{I2} \cdot \alpha \cdot \gamma + K_{I2} \cdot \gamma \cdot [I] + [I]^2} \quad (\text{Eq. 2a})$$

and the dependence of  ${}^{obs}k_{cat}$  on inhibitor **1c** concentration  $[I]$  can be described by Eq. (2b)

$${}^{obs}k_{cat} = {}^0k_{cat} \cdot \frac{K_{I1} \cdot K_{I2} \cdot \alpha \cdot \gamma + K_{I2} \cdot \beta \cdot \gamma \cdot [I] + \delta \cdot [I]^2}{K_{I1} \cdot K_{I2} \cdot \alpha \cdot \gamma + K_{I2} \cdot \gamma \cdot [I] + [I]^2} \quad (\text{Eq. 2b})$$

where  ${}^{obs}K_m$  and  ${}^{obs}k_{cat}$  are the parameters obtained, at a given inhibitor **1c** concentration, from the analysis of the substrate concentration dependence according to Eq. 1, whereas  ${}^0K_m$  and  ${}^0k_{cat}$  are the catalytic parameters obtained in the absence of the inhibitor **1c**. From data reported in Figure 2C it emerged that inhibitor **1c** binds with high affinity ( $K_{I1} = 11 \pm 4$  nM) to a first site, inducing a dramatic 200-fold decrease of the substrate affinity (as from  $\alpha = 190$ , see Figure 2C).

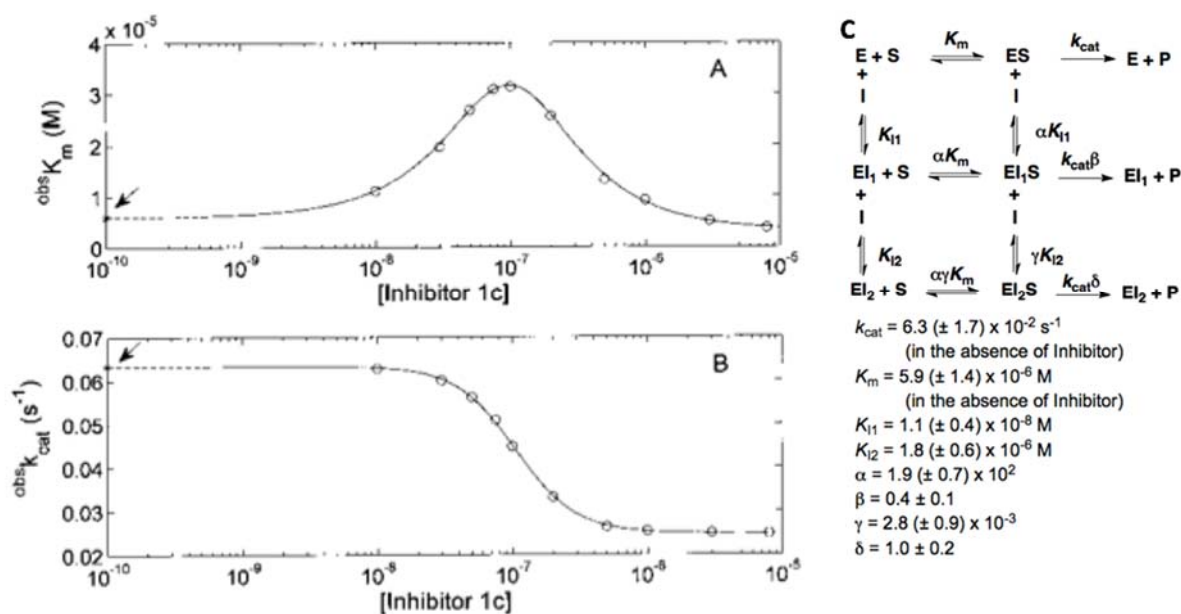


**Figure 2.** (A,B) Dependence on inhibitor **1c** concentration for the values of  ${}^{obs}K_m$  (A) and  ${}^{obs}k_{cat}$  (B); error bars are within the size of the symbols. Continuous lines correspond to the global non-linear least-squares fitting of data according to Eqs 2a and 2b, employing parameters reported in (C). Arrows indicate the values in the absence of Inhibitor; (C) Thermodynamic equilibria for the enzyme, substrate and inhibitor interactions and parameters obtained according to the reported scheme, where E, S and I refer to the enzyme, substrate and inhibitor **1c**, respectively;  $K_m$  and  $k_{cat}$  refer to the Michaelis-Menten equilibrium constant and to the velocity of the rate-limiting step, respectively, in the absence of inhibitor;  $K_{I1}$  and  $K_{I2}$  refer to the equilibrium dissociation constants of inhibitor **1c** for the two binding sites on the enzyme;  $\alpha$  is the interaction parameter for the affinity (reflecting the effect of the inhibitor **1c** on the substrate affinity and/or the effect of substrate on the inhibitor affinity, with:  $\alpha < 1$  representing a positive interaction, which increases the substrate and/or inhibitor affinity;  $\alpha > 1$  representing a negative interaction, which decreases the substrate and/or inhibitor affinity;  $\alpha = 1$  no interaction), and  $\beta$  is the interaction parameter for the rate-limiting step (reflecting the effect of the inhibitor binding on  $k_{cat}$ , with:  $\beta < 1$  representing a negative interaction, which decreases the rate of substrate proteolytic cleavage;  $\beta > 1$  representing a positive interaction, which increases the rate of substrate enzymatic processing;  $\beta = 1$  no interaction). Parameters  $\gamma$  and  $\delta$  have the same meaning, referring to the second binding site of the inhibitor **1c**.

This behavior is similar to that of a competitive inhibitor, but we also observed an effect on  $k_{\text{cat}}$ , which undergoes a 40% reduction (as indicated by  $\beta = 0.4$ , see Figure 2C and Figure 2B); therefore, the inhibitor action should be defined as a mixed inhibition. In any case, the value of  $K_{i1}$  allows to assess that, to our knowledge, this is by far the most powerful inhibitor of Zmp1,<sup>[14]</sup> even more than phosphoramidon, being already active at a concentration of 10 nM.<sup>[9]</sup> A second binding site for inhibitor **1c** is observed upon further increase of inhibitor concentration (micromolar range), which is characterized by  $K_{i2} = 1.8 \pm 0.6 \mu\text{M}$ . Binding to this second site displays an activation effect on the enzymatic activity of Zmp1, which can be attributed only to an increase of substrate affinity; this second binding site, which is very likely to be located far from the active site of Zmp1, acts as an allosteric site, possibly inducing a conformational change of the active site, which increases the substrate affinity (though not facilitating the substrate cleavage). However, the concentration range within which this second binding site becomes operative is 100-fold higher than for the first site, making it much less relevant from the functional viewpoint; however, the detection of this second activating site is important, since it envisages the possibility that an exceedingly high local concentration of the inhibitor **1c** might induce a paradoxical effect by activating the enzymatic activity of Zmp1, partially annihilating the strong inhibitory effect after the binding to the first site at the catalytic center (see Figures 2A and 2B).

### Structure-activity relationships and molecular modeling

The  $\text{IC}_{50}$  values of the inhibitors reported in Table 1 clearly indicate that an intact 8-hydroxy-2-quinolyl-hydroxamate fragment, as in compounds **1a-e**, is necessary to achieve potent Zmp1 inhibition, while the O-alkyl substituent finely tunes the inhibition potency. All modifications of **1c** affecting moieties of the molecule potentially involved in the interaction with the zinc ion, as in compounds **2a,b** and **5a,b**, resulted in a dramatic drop of potency (Table 1). The lack of activity of compounds **3** and **4** (clioquinol) highlight the importance of the side chain attached to the hydroxamate moiety for a correct interaction with the enzyme binding site. In order to assess the binding mode of **1c** and to explain the SARs observed for the class of compounds here described we performed a computational analysis by applying a docking procedure.<sup>[16, 17]</sup> Given the characteristics of the cavity and the presence of a charged metal ion in the binding site, we used the QM-Polarized Ligand Docking (QPLD)<sup>[18-20]</sup> protocol as detailed in materials and methods. The resulting docking pose is reported in Figure 3A for the most potent inhibitor **1c**.

The carbonyl group of **1c** is lodged at an appropriate distance (2.2 Å) to form a metal-coordination bond with  $\text{Zn}^{2+}$ , while the remaining heteroatoms form productive interactions with neighboring residues in the active site pocket explaining the observed SAR. In particular, the 8-OH group of **1c** establishes an H-bond with E560, the carbonyl group, and the endocyclic nitrogen forms two H-bond interactions with H622; the hydroxamate NH interacts with N452, and finally, the hydroxamate oxygen is involved in H-bond with R628. Hydrophobic contacts, such as  $\pi$ - $\pi$  stacking of the benzyl ring with H493, W604 and F48 (S1' site) and of the hydroxyquinoline with H622 further stabilize the observed binding pose. The

dramatic drop of inhibitory potency observed for the isosteric compound **2a**, bearing a methylene in place of the hydroxamate oxygen (**2a** vs **1c**, Table 1), prompted us to further investigate its binding mode (Figure 3B). Compound **2a**, lacking the oxygen atom, fails to interact with R628, so cannot correctly accommodate its carbonyl group close to the zinc ion. The lack of appropriate metal-coordination results in a large portion of the 8-hydroxyquinoline moiety solvent exposed towards the *lumen* of the big cavity of Zmp1. Remarkably, these different binding modes found for **1c** and **2a** by means of QPLD protocol, were in agreement with the estimated ligand binding energy ( $\Delta G_{\text{bind}}$ , -77.53 kcal/mol and of -40.01 kcal/mol for **1c** and **2a** respectively).

The QPLD protocol was also applied to compound **4** and results are consistent with its lack of inhibitory activity at the highest concentration tested (Figure S4 of the Supporting Information file).

### Evaluation of the activity of Zmp1 inhibitor **1c** against *M. tuberculosis* in macrophages

As a preliminary evaluation, the anti-mycobacterial activity of the most potent inhibitor of Zmp1 (compound **1c**) was tested during intracellular infection of *M. tuberculosis* in J774 murine macrophages (Figure 4A). We chose a low MOI (1:10) since at higher MOI Mtb cause toxicity early after infection. Moreover, the drug was added 24 h post infection to allow the activation of the Mtb evasion strategies inside the macrophages.

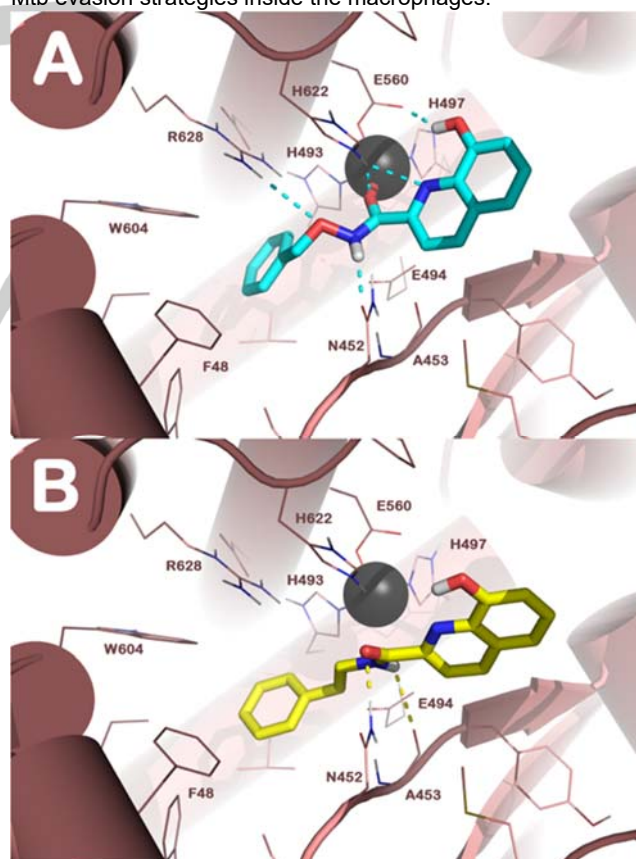


**Figure 3.** QPLD pose of **1c** (A) and **2a** (B) into Zmp1 binding site (PDB ID: 3ZUK). The pictures were generated by means of PyMOL (The PyMOL Molecular Graphics System, version 1.6-alpha, Schrödinger, LLC, New York, 2013).

Compound **1c**, tested at 6.5  $\mu\text{g/mL}$  concentration, caused a reduction in treated vs control of  $-0.63 \text{ LogCFU}/10^6 \text{ cells}$ . Conversely, no effect on the viability of the avirulent strain *M. bovis* BCG in J774 macrophages was observed for compound **1c** at a concentration of 6.5  $\mu\text{g/mL}$  (Figure 4B), despite the fact that a MOI of 5:1 was used. Previous studies showed that deletion of the *zmp1* gene affected intracellular survival of both *M. tuberculosis* and *M. bovis* BCG, though the impact on the latter was much less dramatic, probably because BCG is strongly attenuated and cannot effectively inhibit phagosome-lysosome fusion.<sup>[7]</sup> Hence, the restricted activity of **1c** for the virulent *M. tuberculosis* strain, but not for BCG, may underscore the different role played by Zmp1 in virulent vs attenuated mycobacterial strains. Notably, no anti-mycobacterial activity was observed for compound **1c** against extracellular *M. tuberculosis* (MIC > 20  $\mu\text{g/mL}$ ) as assessed by determination of the minimal inhibitory concentration in axenic culture (data not shown): the result is consistent with the previously reported lack of effects on *M. tuberculosis* viability in axenic culture following Zmp1 deletion.<sup>[7]</sup> Given these promising preliminary results, evaluation on *M. tuberculosis*-infected human monocyte-derived macrophages (hMDM) was subsequently performed (Figure 4C). Compound **1c** showed antibacterial activity against virulent *M. tuberculosis* in human primary macrophages (**1c** added at day 1 p.i.) in a dose-dependent manner. In fact, **1c** caused  $-0.56$ ,  $-0.42$  and  $-0.34$  reduction in  $\text{logCFU}/10^6 \text{ cells}$  in treated vs control hMMD, at

doses of 20, 6.5 and 2.5  $\mu\text{g/mL}$ , respectively. At the highest dose tested, the effect of **1c** was comparable to that of the second-line antitubercular drug capreomycin (added at the concentration of 4  $\mu\text{g/mL}$ ), an important second-line drug currently used for the treatment of MDR-TB. A similar effect was also observed when **1c** was added immediately after infection (at 4 hpi, see Figure S5 of the Supporting Information file). Cytotoxicity of **1c** on hMDM was subsequently assessed and resulted in a 10% cell mortality, comparable to that the untreated control, even at the highest concentration of 20  $\mu\text{g/mL}$  (Figure 5). Notably, at the same molar concentration compound **4**, a Zn-complexing agents with no inhibitory activity on Zmp1, resulted in 57% toxicity.

### In Vitro Toxicity and Genotoxicity Assays

The drug-like properties of **1c** were further investigated by determining cytotoxicity *in vitro* on mouse fibroblasts NIH3T3. A  $\text{TC}_{50}$  value of 54  $\mu\text{M}$  was indicative of an optimal selectivity index ( $\text{SI} \approx 5000$ ). Investigation of the mutagenic potential of **1c** was assayed in the *Salmonella typhimurium* strains TA98 and TA100 using the Ames test (Figure S6 of the Supporting Information),<sup>[17]</sup> indicating that **1c** was not mutagenic over the concentration range tested.

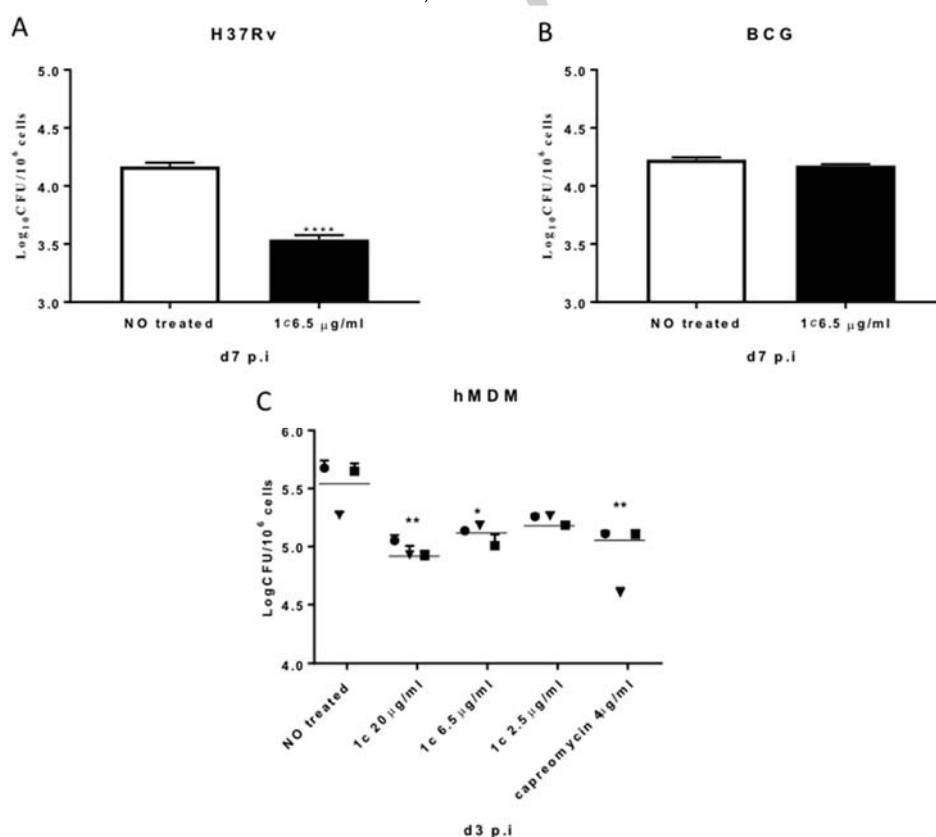


**Figure 4.** J774 murine macrophages were infected with (A) *M. tuberculosis* H37Rv (MOI of 1:10) and (B) *M. bovis* BCG (MOI 5:1). Intracellular bacteria were determined by CFU counting at day 7 post-infection. Results of one representative experiment of at least three assays are shown. Statistical analysis was performed with 2-way ANOVA with Bonferroni's posttest; (C) Human monocyte-derived macrophages (hMDM) were infected with *M. tuberculosis* H37Rv (MOI of 1:1) and incubated with the test drug for 3 days post-infection. Intracellular bacteria were evaluated by CFU counts. The result shown derive from hMDM obtained from three different donors, each tested in triplicate. Statistical significance was determined by One-way ANOVA, Dunnett's multiple comparison test.

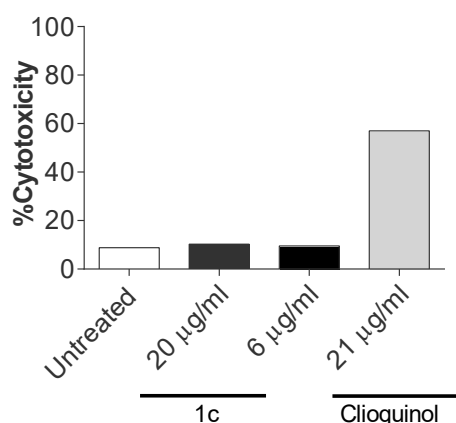


**Figure 5.** Cytotoxicity was tested with the CytoTox 96<sup>®</sup> Non-Radioactive Cytotoxicity Assay kit (Promega) according to manufacturer's instructions.

## Conclusions

In conclusion, Zmp1 has been claimed as a putative and novel target for development of potential anti-TB drugs.<sup>[6, 7]</sup> However, its role in mycobacterium survival is still under debate.<sup>[8]</sup> We described herein the development of a series of potent inhibitors of Zmp1. Quinoline **1c** was used as a pharmacological tool in an attempt to clarify the biological role of Zmp1. **1c** was able to impair survival of *M. tuberculosis* in human primary macrophages in a dose-dependent manner when administered at both 24 and 4 h p.i. Further work is needed to confirm that zmp1 is the intracellular target of **1c**, but these preliminary data indicate that the role of Zmp1 in protecting *M. tuberculosis* from the host immune system is worth of further investigation.

## Experimental Section

### Chemistry

**General:** Reagents were purchased from Aldrich and were used as received. Reaction progress was monitored by TLC using Merck silica gel 60 F254 (0.040–0.063 mm) with detection by UV. Merck silica gel 60 (0.040–0.063 mm) was used for column chromatography. Melting points were determined in Pyrex capillary tubes using an Electrothermal 8103 or Gallenkamp apparatus and are uncorrected. <sup>1</sup>H NMR and <sup>13</sup>C NMR spectra were recorded on Varian 300 MHz or Bruker 400 MHz spectrometers by using the residual signal of the deuterated solvent as internal standard. Splitting patterns are described as singlet (s), doublet (d), triplet (t), quartet (q), and broad (br); the value of chemical shifts ( $\delta$ ) are given in ppm and coupling constants (*J*) in Hertz (Hz). ESI-MS spectra were performed by an Agilent 1100 Series LC/MSD spectrometer. RP-HPLC was performed on a Shimadzu Prominence apparatus equipped with LC-20AD pump, SIL-20AC HT autosampler, CTO-20AC column oven and SPD-M20A diode array detector. The purity of all compounds tested was  $\geq$  96% as determined by RP-HPLC (RP-18 Chromolith column, 4.6 mm diameter; gradient elution: solvent A: 1% TFA in ACN, solvent B: 0.5% TFA in H<sub>2</sub>O, from 20 to 70% solvent A in 6 min, UV detection: 254 nm).

**General Procedure for the synthesis of 1a-e, 2a,b and 3a,b:** 1-Hydroxybenzotriazole (0.58 mmol) and 1-ethyl-3-(3-dimethylaminopropyl)carbodiimide (0.57 mmol) were added to a mixture of the appropriate 2-carboxyquinoline **3** or **9a,b**<sup>[21]</sup> (0.53 mmol) and *N*-

methylmorpholine (0.57 mmol) in *N,N*-dimethylformamide (5.0 mL). The resulting mixture was stirred at 25 °C for 2 h, afterward the appropriate hydroxylamine **6a-e** or amine **7a,b** (0.79 mmol) was added and stirring was continued overnight. The mixture was partitioned between water and dichloromethane and the organic layer was washed with water, dried over sodium sulfate, and concentrated *in vacuo*.

***N*-Methoxy-8-hydroxyquinoline-2-carboxamide (1a):** Brown solid (yield 35%, Mp 201–202 °C). <sup>1</sup>H NMR (400 MHz, CDCl<sub>3</sub>)  $\delta$  3.97 (s, 3H), 7.24 (d, *J* = 7.8 Hz, 1H), 7.41 (d, *J* = 8.3 Hz, 1H), 7.56 (t, *J* = 7.9 Hz, 1H), 7.73 (br s, 1H), 8.28–8.35 (m, 2H), 10.30 (br s, 1H). MS (ESI) *m/z* 241 [M + Na]<sup>+</sup>. HPLC purity: 96.9% (*R*<sub>t</sub> = 4.031 min).

***N*-(Allyloxy)-8-hydroxyquinoline-2-carboxamide (1b):** Flash chromatography: dichloromethane-methanol (95:5) (62% yield). An analytical sample was obtained by recrystallization from diethyl ether-*n*-hexane by slow evaporation as a pale-yellow crystalline solid (Mp 121–122 °C). <sup>1</sup>H NMR (400 MHz, CDCl<sub>3</sub>)  $\delta$  4.57 (d, *J* = 6.5 Hz, 2H), 5.26–5.37 (m, 2H), 5.99–6.09 (m, 1H), 7.24 (d, *J* = 7.7 Hz, 1H), 7.39 (d, *J* = 8.2 Hz, 1H), 7.50–7.58 (m, 1H), 8.03 (br s, 1H), 8.23–8.37 (m, 2H), 10.58 (br s, 1H). MS (ESI) *m/z* 245 [M + H]<sup>+</sup>. HPLC purity: 96.6% (*R*<sub>t</sub> = 4.950 min).

***N*-(Benzyloxy)-8-hydroxyquinoline-2-carboxamide (1c):** Flash chromatography: dichloromethane-methanol (98:2) (yield 77%). An analytical sample was obtained by recrystallization from diethyl ether-*n*-hexane as pale-yellow crystals melting at 143–144 °C. <sup>1</sup>H NMR (400 MHz, CDCl<sub>3</sub>)  $\delta$  5.09 (s, 2H), 7.21 (d, *J* = 7.6 Hz, 1H), 7.35–7.46 (m, 6H), 7.53 (t, *J* = 7.8 Hz, 1H), 7.78 (br s, 1H), 8.30–8.32 (m, 2H), 10.35 (br s, 1H). <sup>13</sup>C NMR (75 MHz, CDCl<sub>3</sub>)  $\delta$  163.2, 153.4, 146.0, 139.0, 138.6, 132.1, 131.7, 130.3, 129.9, 129.1, 128.7, 128.0, 126.5, 121.8, 119.7, 112.0, 79.8; MS (ESI) *m/z* 295 [M + H]<sup>+</sup>, 317 [M + Na]<sup>+</sup>. HPLC purity: 99.9% (*R*<sub>t</sub> = 6.196 min).

***N*-(4-Methylbenzyloxy)-8-hydroxyquinoline-2-carboxamide (1d):** Flash-chromatography: dichloromethane-methanol (98:2) (yield 63%). An analytical sample was obtained by recrystallization from diethyl ether-*n*-hexane by slow evaporation as colorless crystals melting at 146–147 °C. <sup>1</sup>H NMR (400 MHz, CDCl<sub>3</sub>)  $\delta$  2.22 (s, 3H), 4.98 (s, 2H), 6.98 (d, *J* = 7.7 Hz, 2H), 7.15–7.22 (m, 3H), 7.33 (t, *J* = 8.3 Hz, 1H), 7.55 (t, *J* = 7.9 Hz, 1H), 8.22–8.28 (m, 2H), 8.49 (br s, 1H), 11.15 (br s, 1H). MS (ESI) *m/z* 309 [M + H]<sup>+</sup>. HPLC purity: 99.5% (*R*<sub>t</sub> = 6.717 min).

***N*-(3,4-Dichlorobenzyloxy)-8-hydroxyquinoline-2-carboxamide (1e):** Flash-chromatography: dichloromethane-methanol (98:2) (yield 66%). Compound **1e** was obtained as a pale-yellow oil, which crystallized on standing (179–180 °C). <sup>1</sup>H NMR (400 MHz, CDCl<sub>3</sub>)  $\delta$  4.97 (s, 2H), 7.15–7.20 (m, 3H), 7.30–7.36 (m, 2H), 7.45 (s, 1H), 7.50 (t, *J* = 7.9 Hz, 1H), 8.22–8.29 (m, 2H), 11.40 (br s, 1H). MS (ESI) *m/z* 363 [M + H]<sup>+</sup>. HPLC purity: 96.5% (*R*<sub>t</sub> = 7.472 min).

***N*-Phenethyl-8-hydroxyquinoline-2-carboxamide (2a):** Flash-chromatography: chloroform-ethyl acetate (8:2). Compound **2a** was obtained as a pale-yellow oil, which crystallized on standing (yield 89%, Mp 171–172 °C). <sup>1</sup>H NMR (400 MHz, CDCl<sub>3</sub>)  $\delta$  2.99 (t, *J* = 6.8 Hz, 2H), 3.80 (q, *J* = 6.7 Hz, 2H), 7.19–7.32 (m, 4H), 7.35–7.43 (m, 3H), 7.49 (s, 1H), 7.53 (t, *J* = 7.9 Hz, 1H), 7.91 (br s, 1H), 8.29–8.34 (m, 2H); MS (ESI) *m/z* 315 [M + Na]<sup>+</sup>. HPLC purity: 100% (*R*<sub>t</sub> = 6.740 min).

***N*-(3-Phenylpropyl)-8-hydroxyquinoline-2-carboxamide (2b):** Flash-chromatography: chloroform-ethyl acetate (9:1). Compound **2b** was obtained as a pale-yellow oil, which crystallized on standing (yield 73%, Mp 106.8–107.2 °C). <sup>1</sup>H NMR (400 MHz, CDCl<sub>3</sub>)  $\delta$  1.99–2.11 (m, 2H), 2.75 (t, *J* = 7.5 Hz, 2H), 3.59 (q, *J* = 6.8 Hz, 2H), 7.13–7.31 (m, 6H), 7.40 (dd, *J* = 8.2, 0.8 Hz, 1H), 7.53 (t, *J* = 7.9 Hz, 1H), 7.70 (s, 1H), 7.87 (br s, 1H), 8.29–8.35 (m, 2H). MS (ESI) *m/z* 307 [M + H]<sup>+</sup>. HPLC purity: 100% (*R*<sub>t</sub> = 7.237 min).

**8-Methoxy-2-quinolylcarboxylic acid (9a):** To a solution of **8** (130 mg, 0.6 mmol), prepared from **5** following a described procedure,<sup>[22]</sup> in MeOH (3 mL) and water (2 mL), lithium hydroxide was added (36 mg, 1.5 mmol). The reaction mixture was stirred at room temperature for 1 h. The solution was filtered on celite to afford the title compound (120 mg, 100%) without further purification as a pale yellow solid. <sup>1</sup>H NMR (400 MHz, DMSO-*d*<sub>6</sub>): δ 3.11 (br s, 1H), 3.96 (s, 3H), 7.22-7.24 (d, *J* = 8.0 Hz, 1H), 7.53-7.60 (m, 2H), 8.04-8.06 (d, *J* = 8.0 Hz, 1H), 8.42-8.44 (d, *J* = 8.0 Hz, 1H); MS (ESI) *m/z* 202 [M - H]<sup>+</sup>.

**8-Methoxy-2-quinolylhydroxamic acid benzyl ester (5a):** White solid (32% yield, Mp 143-144 °C). <sup>1</sup>H NMR (400 MHz, CDCl<sub>3</sub>): δ 8.27 (d, *J* = 8.5 Hz, 1H), 8.21 (d, *J* = 8.5 Hz, 1H), 7.62 – 7.50 (m, 1H), 7.42 (d, *J* = 8.3 Hz, 1H), 7.39 – 7.25 (m, 4H), 7.08 (d, *J* = 7.8 Hz, 1H), 5.05 (s, 2H), 4.04 (s, 3H); MS (ESI) *m/z* 279 [M + H]<sup>+</sup>, 301 [M + Na]<sup>+</sup>, 579 [2M + Na]<sup>+</sup>.

**2-Quinolylhydroxamic acid benzyl ester (5b):** White solid (25% yield, Mp 157-158 °C). <sup>1</sup>H NMR (400 MHz, CDCl<sub>3</sub>): δ 5.10 (s, 2H), 7.34-7.41 (m, 3H), 7.48-7.50 (d, *J* = 8.0 Hz, 2H), 7.58-7.61 (t, *J* = 3.04 Hz, 1H), 7.70-7.74 (t, *J* = 16 Hz, 1H), 7.83-7.85 (d, *J* = 8.0 Hz, 1H), 7.98-8.00 (d, *J* = 8.0 Hz, 1H), 8.08-8.31 (m, 2H), 10.35 (brs, 1H); <sup>13</sup>C NMR (75 MHz, CDCl<sub>3</sub>): δ 162.2, 149.0, 148.5, 137.9, 135.4, 132.5, 132.1, 131.7, 131.2, 130.3, 129.9, 129.1, 128.7, 128.0, 126.5, 119.0, 79.6. HPLC purity: 97.8% (R<sub>t</sub> = 6.529 min).

**X-Ray Crystallography:** Single crystals of compounds **1b-d** (VC1602, VC1222, VC1620) were submitted to X-ray data collection on an Oxford-Diffraction Xcalibur Sapphire 3 diffractometer with a graphite monochromated Mo-K $\alpha$  radiation ( $\lambda$  = 0.71073 Å) at 293 K. The structures were solved by direct methods implemented in SHELXS-97 program.<sup>[23]</sup> The refinements were carried out by full-matrix anisotropic least-squares on F<sup>2</sup> for all reflections for non-H atoms by means of the SHELXL-97 program.<sup>[24]</sup> Crystallographic data (excluding structure factors) for the structure in this paper have been deposited with the Cambridge Crystallographic Data Centre as supplementary publication no. CCDC 1062834 (**1b**), 1062832 (**1c**), and 1062835 (**1d**). Copies of the data can be obtained, free of charge, on application to CCDC, 12 Union Road, Cambridge CB2 1EZ, UK; (fax: + 44 (0) 1223 336 033; or e-mail: [deposit@ccdc.cam.ac.uk](mailto:deposit@ccdc.cam.ac.uk)).

### Computational details

**Protein and ligands preparation:** All ligands were built and treated by means of Maestro<sup>[25]</sup> software as described previously.<sup>[26-28]</sup> The compounds were filtered for pan assay interference compounds (PAIS). None of them contained sub-structural features that would label them as “frequent hitters” in high throughput screens.<sup>[29]</sup> The three-dimensional structure of Zmp1 (PDB ID 3ZUK) was taken from PDB, imported into Maestro and prepared as described previously.<sup>[30, 31]</sup>

**QM-Polarized Ligand Docking (QLPD), ligand binding energies:** Docking studies were performed employing the QPLD workflow implemented in Maestro.<sup>[18, 20]</sup> QLPD utilizes Glide and Qsite software to carry out the calculation for performing docking studies using *ab initio* methodology to calculate ligand charges within the protein environment, which is essential for charged active sites, such as metalloproteinase. QPLD improves the partial charges on the ligand atoms in Glide docking run by replacing them with charges generated from a quantum-mechanical (QM) calculation on the ligand in the field of the receptor. Energy grids were prepared using default settings within a cubic box centered on the Zn<sup>2+</sup> atom. Initial ligands charges were generated adopting a semi-empirical method. Ligands were docked using Glide Extra Precision (XP). QM charges were calculated by using Jaguar<sup>[32]</sup> from the electrostatic potential energy surface of the ligand, which is generated from a single point calculation using DFT for the QM region at 6-31G\*/LACVP\* basis set, B3LYP density function. The generated poses were re-docked employing XP method applying the calculated QM charges. Resulting post-docking minimized poses were scored and ranked by Glide XP. The binding energies were estimated using Prime MM-GBSA for the complexes **1c-**

Zmp1 and **2a-Zmp1** as described previously.<sup>[33-35]</sup>

### Biological evaluation

**Kinetic analysis of Zmp1 inhibition:** Synthesized compounds underwent a preliminary screening in order to identify the lead compound. Briefly, 10  $\mu$ M inhibitor was preincubated with 0.5 nM Zmp1 in the reaction buffer (100 mM Tris-HCl, 0.1% borate, 150 mM NaCl, and 10 mM CaCl<sub>2</sub>, pH 8.0) for 15 min at 37 °C. Thereafter a fluorogenic substrate for the enzyme was added to the reaction mixture. Notably, the MMP2/MMP7 fluorogenic substrate displays the aminoacid sequence PLGL flanked by the fluorophore/quencher system methoxycoumarin/dinitrophenyl-alanine-arginine (full sequence: MCA-Pro-Leu-Gly-Leu-Dpa-Ala-Arg-NH<sub>2</sub>; MCA stands for (7-methoxycoumarin-4-yl)-acetyl; Dpa stands for N-3-(2,4-dinitrophenyl)-L-2,3-diaminopropionyl. MCA is the fluorophore, Dpa the quencher (MMP2/MMP7 product number 03-32-5032, Calbiochem). MMP2/MMP7 was shown to be efficiently cleaved by Zmp1 *in vitro*.<sup>[9, 10]</sup> The compounds (indicated in Figure 1B) with significant inhibitory properties were further assayed at different concentrations (ranging from 100 nM to 50  $\mu$ M) in order to obtain the IC<sub>50</sub>. In addition, for compound **1c**, which displayed the highest inhibitory properties (see Figure 1B), kinetic analysis to determine K<sub>i</sub> was performed, as indicated below: several **1c** concentrations, ranging from 0.5 to 250 nM, were pre-incubated with 0.5 nM Zmp1. Afterwards, the fluorogenic substrate was added at a concentration ranging from 1  $\mu$ M to 50  $\mu$ M. The analysis of the inhibitory properties of compound **1c** on MMP-2 and MMP-1 was performed according to the following experimental conditions: **1c** at various concentrations, ranging from 50 nM to 50  $\mu$ M, was preincubated for 15 min at 37 °C with either 10 nM MMP-2 or 10 nM MMP-1 in the reaction buffer (50 mM Tris-HCl, 10 mM CaCl<sub>2</sub>, 100 mM NaCl, pH 7.5). Thereafter, an omni-MMP fluorogenic substrates was added at a final concentration of 20  $\mu$ M (Calbiochem). In all cases, the substrate hydrolysis was recorded in an Eclipse fluorometer (Varian) (excitation 320 nm, emission 395 nm) and the reaction was followed until linearity was observed.

**In vitro biological assay of 1c:** J774 murine macrophages were cultured in 48-well plates as previously indicated,<sup>[36]</sup> and infected with *M. tuberculosis* H37Rv or with *M. bovis* BCG at a multiplicity of infection (MOI) of 1:10 and 5:1, respectively. Following a 2 h infection, the infecting solution were removed and cells were washed three times with PBS, remove extracellular bacteria, and then incubated with maintaining medium (2% fetal bovine serum). 24 h post-infection, compound **1c** was added to the infected cells at different concentrations. As a control, cells infected with both *M. tuberculosis* H37Rv and with *M. bovis* BCG received 0  $\mu$ g/mL of compound **1c**. At day 7 post-infection, cells were washed three times with PBS, lysed in 0.1% Triton X-100 and intracellular bacteria were determined by colony forming units (CFUs) counting by serially diluting lysates in PBS containing 0.05% Tween80 and plating on 7H11 OADC 0.05% Tween80 agar plates.<sup>[37]</sup> Colony counting was performed in triplicate. A similar protocol was applied to human monocyte-derived macrophages (*hMDM*) with a few changes. Briefly, peripheral blood mononuclear cells (PBMCs) were isolated from buffy coats of 3 male donors by using Ficoll (Cedarlane) and were processed to collect *hMDMs* by positive selection from the PBMCs suspension by using CD14 MicroBeads, following the manufacturer's instructions (Miltenyi Biotec). *hMDMs* were seeded at 1.2 · 10<sup>6</sup> cells/ml in 48-well plates in X-VIVO<sup>TM</sup> 15 medium (Lonza) with human serum type AB 2% (Lonza), and incubated for 6-7 days at 37°C in a 5% humidified atmosphere until *hMDM* differentiation. No antibiotics were added to the medium. Adhered macrophages were infected with *Mtb* H37Rv strain at a MOI of 1:1. As described for J774 cells, *hMDMs* were infected and intracellular mycobacterial CFUs were determined at 4 h and 72 h post-infection.<sup>[36]</sup> Compound **1c** was added 24h post infection at different concentrations (20, 6.5, 2.5  $\mu$ g/mL) while we added a second line anti-TB drug capreomycin 4  $\mu$ g/mL as positive control. Each condition was tested in triplicate.

**Toxicity and Ames test:** The toxicity evaluation against NIH3T3 fibroblasts and Ames test were performed as previously described

following literature procedures.<sup>[17, 38, 39]</sup> Cytotoxicity on human macrophages was tested with the CytoTox 96<sup>®</sup> Non-Radioactive Cytotoxicity Assay kit (Promega) according to manufacturer's instructions.

## Acknowledgements

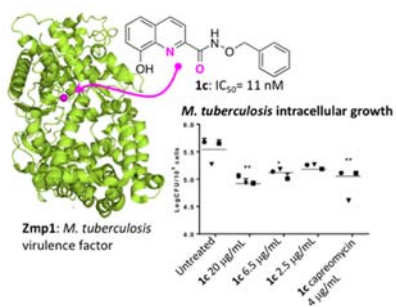
Authors thank Prof. Menico Rizzi for plasmids of Zmp1. This work was supported by the Italian Ministry of University and Research (MiUR PRIN 200993WWF9 to M.C. and M. A.) and by the British Society for Antimicrobial Chemotherapy (BSAC RESEARCH GRANT 2016 grant number GA2016\_087R to S. Brogi)

**Keywords:** 8-hydroxyquinoline-2-hydroxamate • metallo-protease inhibitors • *Mycobacterium tuberculosis* • QPLD • zmp1

## References:

- [1] WHO, in p. Global tuberculosis report 2016.
- [2] C. Lange, I. Abubakar, J. W. Alffenaar, G. Bothamley, J. A. Caminero, A. C. Carvalho, K. C. Chang, L. Codecasa, A. Correia, V. Crudu, P. Davies, M. Dedicoat, F. Drobniewski, R. Duarte, C. Ehlers, C. Erkens, D. Goletti, G. Gunther, E. Ibraim, B. Kampmann, L. Kuksa, W. de Lange, F. van Leth, J. van Lunzen, A. Matteelli, D. Menzies, I. Monedero, E. Richter, S. Rusch-Gerdes, A. Sandgren, A. Scardigli, A. Skrahina, E. Tortoli, G. Volchenkov, D. Wagner, M. J. van der Werf, B. Williams, W. W. Yew, J. P. Zellweger, D. M. Cirillo, *Tbnet, Eur Respir J* **2014**, *44*, 23-63.
- [3] H. A. Blair, L. J. Scott, *Drugs* **2015**, *75*, 91-100.
- [4] M. V. Worley, S. J. Estrada, *Pharmacotherapy* **2014**, *34*, 1187-1197.
- [5] M. A. Forrellad, L. I. Klepp, A. Gioffre, J. Sabio y Garcia, H. R. Morbidoni, M. de la Paz Santangelo, A. A. Cataldi, F. Bigi, *Virulence* **2013**, *4*, 3-66.
- [6] V. Lazarevic, F. Martinon, *Cell Host Microbe* **2008**, *3*, 199-200.
- [7] S. S. Master, S. K. Rampini, A. S. Davis, C. Keller, S. Ehlers, B. Springer, G. S. Timmins, P. Sander, V. Deretic, *Cell Host Microbe* **2008**, *3*, 224-232.
- [8] D. G. Muttucumar, D. A. Smith, E. J. McMin, V. Reese, R. N. Coler, T. Parish, *Tuberculosis (Edinb)* **2011**, *91*, 111-116.
- [9] D. M. Ferraris, D. Sbardella, A. Petrer, S. Marini, B. Amstutz, M. Coletta, P. Sander, M. Rizzi, *J. Biol. Chem.* **2011**, *286*, 32475-32482.
- [10] A. Petrer, B. Amstutz, M. Gioia, J. Hahnlein, A. Baici, P. Selchow, D. M. Ferraris, M. Rizzi, D. Sbardella, S. Marini, M. Coletta, P. Sander, *Biol. Chem.* **2012**, *393*, 631-640.
- [11] M. H. Vemula, R. Ganji, R. Sivangala, K. Jakkala, S. Gaddam, S. Penmetsa, S. Banerjee, *Front. Microbiol.* **2016**, *7*, 418.
- [12] J. A. Jacobsen, J. L. Major Jourden, M. T. Miller, S. M. Cohen, *Biochim. Biophys. Acta* **2010**, *1803*, 72-94.
- [13] Y. Song, H. Xu, W. Chen, P. Zhan, X. Liu, *Med. Chem. Commun.* **2015**, *6*, 61-74.
- [14] M. Mori, F. Moraca, D. Deodato, D. M. Ferraris, P. Selchow, P. Sander, M. Rizzi, M. Botta, *Bioorg. Med. Chem. Lett.* **2014**, *24*, 2508-2511.
- [15] D. Sbardella, G. F. Fasciglione, M. Gioia, C. Ciaccio, G. R. Tundo, S. Marini, M. Coletta, *Mol. Aspects Med.* **2012**, *33*, 119-208.
- [16] S. Giovani, M. Penzo, S. Brogi, M. Brindisi, S. Gemma, E. Novellino, M. J. Blackman, G. Campiani, S. Butini, *Bioorg. Med. Chem. Lett.* **2014**, *24*, 3582-3586.
- [17] S. Gemma, C. Camodeca, M. Brindisi, S. Brogi, G. Kukreja, S. Kunjir, E. Gabellieri, L. Lucantoni, A. Habluetzel, D. Taramelli, N. Basilio, R. Gualdani, F. Tadini-Buoninsegni, G. Bartolommei, M. R. Moncelli, R. E. Martin, R. L. Summers, S. Lamponi, L. Savini, I. Fiorini, M. Valoti, E. Novellino, G. Campiani, S. Butini, *J. Med. Chem.* **2012**, *55*, 10387-10404.
- [18] A. E. Cho, V. Guallar, B. J. Berne, R. Friesner, *J. Comput. Chem.* **2005**, *26*, 915-931.
- [19] A. E. Cho, D. Rinaldo, *J. Comput. Chem.* **2009**, *30*, 2609-2616.
- [20] Schrödinger, Suite 2011 QM-Polarized Ligand Docking protocol; Glide version 2015.2017, Schrödinger, LLC, New York, NY, 2011; Jaguar version 2017.2018, Schrödinger, LLC, New York, NY, 2011; QSite version 2015.2017, Schrödinger, LLC, New York, NY, 2011.
- [21] R. H. Dodd, M. Lehyaric, *Synthesis* **1993**, 295-297.
- [22] A. N. Pearce, E. W. Chia, M. V. Berridge, G. R. Clark, J. L. Harper, L. Larsen, E. W. Maas, M. J. Page, N. B. Perry, V. L. Webb, B. R. Copp, *J. Nat. Prod.* **2007**, *70*, 936-940.
- [23] G. M. Sheldrick.
- [24] G. M. Sheldrick.
- [25] Maestro, 9.2 ed. (Ed.: 9.2), Schrödinger, LLC, New York, NY, 2011, **2011**.
- [26] M. Brindisi, S. Maramai, S. Gemma, S. Brogi, A. Grillo, L. D. Mannelli, E. Gabellieri, S. Lamponi, S. Saponara, B. Gorelli, D. Tedesco, T. Bonfiglio, C. Landry, K. M. Jung, A. Armirotti, L. Luongo, A. Ligresti, F. Piscitelli, C. Bertucci, M. P. Dehouck, G. Campiani, S. Malone, C. Ghelardini, A. Pittaluga, D. Piomelli, V. Di Marzo, S. Butini, *J. Med. Chem.* **2016**, *59*, 2612-2632.
- [27] A. Gasser, S. Brogi, K. Urayama, T. Nishi, H. Kurose, A. Tafi, N. Ribeiro, L. Desaubry, C. G. Nebigil, *PLoS One*, *10*, e0121027.
- [28] M. Y. Wu, G. Esteban, S. Brogi, M. Shionoya, L. Wang, G. Campiani, M. Unzeta, T. Inokuchi, S. Butini, J. Marco-Contelles, *Eur. J. Med. Chem.* **2016**.
- [29] J. B. Baell, G. A. Holloway, *J. Med. Chem.* **2010**, *53*, 2719-2740.
- [30] M. Brindisi, S. Giovani, S. Gemma, S. Lamponi, F. De Luca, E. Novellino, G. Campiani, J. D. Docquier, S. Butini, *J. Enzyme Inhib. Med. Chem.* **2016**, 1-12.
- [31] S. Brogi, S. Giovani, M. Brindisi, S. Gemma, E. Novellino, G. Campiani, M. J. Blackman, S. Butini, *J. Mol. Graph. Model.* **2016**, *64*, 121-130.
- [32] Jaguar, 7.8 ed., Schrödinger, LLC, New York, NY, **2011**.
- [33] M. Brindisi, S. Butini, S. Franceschini, S. Brogi, F. Trotta, S. Ros, A. Cagnotto, M. Salmona, A. Casagni, M. Andreassi, S. Saponara, B. Gorelli, P. Weikop, J. D. Mikkelsen, J. Scheel-Kruger, K. Sandager-Nielsen, E. Novellino, G. Campiani, S. Gemma, *J. Med. Chem.* **2014**, *26*, 9575-9597.
- [34] M. Brindisi, S. Gemma, S. Kunjir, L. Di Cerbo, S. Brogi, S. Parapini, S. D'Alessandro, D. Taramelli, A. Habluetzel, S. Tapanelli, S. Lamponi, E. Novellino, G. Campiani, S. Butini, *Medchemcomm* **2015**, *6*, 357-362.
- [35] M. Chioua, M. Perez, O. M. Bautista-Aguilera, M. Yanez, M. G. Lopez, A. Romero, R. Cacabelos, R. P. de la Bellacasa, S. Brogi, S. Butini, J. I. Borrell, J. Marco-Contelles, *Mini Rev. Med. Chem.*, *15*, 648-658.
- [36] I. Palucci, S. Camassa, A. Cascioferro, M. Sali, S. Anosheh, A. Zumbo, M. Minerva, R. Iantomasi, F. De Maio, G. Di Sante, F. Ria, M. Sanguinetti, G. Palu, M. J. Brennan, R. Manganelli, G. Delogu, *PLoS One* **2016**, *11*, e0150800.
- [37] A. Zumbo, I. Palucci, A. Cascioferro, M. Sali, M. Ventura, P. D'Alfonso, R. Iantomasi, G. Di Sante, F. Ria, M. Sanguinetti, G. Fadda, R. Manganelli, G. Delogu, *Pathog. Dis.* **2013**, *69*, 232-239.
- [38] S. Gartiser, C. Hafner, K. Kronenberger-Schafer, O. Happel, C. Trautwein, K. Kummerer, *Environ. Sci. Pollut. Res. Int.* **2012**, *19*, 3597-3609.
- [39] L. G. Nunes, D. C. Gontijo, C. J. Souza, L. G. Fietto, A. F. Carvalho, J. P. Leite, *Environ. Toxicol. Pharmacol.* **2012**, *33*, 297-303.

## Entry for the Table of Contents



Starting from the 8-hydroxyquinoline privileged structure, we designed a series of inhibitors of the metallo-protease enzyme Zmp1. This protease is a virulence factor that allows *Mycobacterium tuberculosis* to survive inside macrophages. The potent inhibitor **1c** is able to impair growth of *M. tuberculosis* inside macrophages and is not active against axenic bacteria.